# NOVEL APPLICATIONS OF MIMO ANTENNA SYSTEM FOR ACTIVE SUPPRESSION OF ELECTROMAGNETIC FIELDS

Tommy Hult och Abbas Mohammed

Blekinge Institute of Technology
Research report No. 2005:11

# Novel Applications of MIMO Antenna System for Active Suppression of Electromagnetic Fields

Tommy Hult and Abbas Mohammed

Research Report
Department of Signal Processing
Ronneby, December 2005

**Abstract**

Active suppression of noise and vibrations is a well established field of research with many applications in acoustic and mechanical industries. In this report we test some of these active control methods combined with MIMO antenna system in order to assess their validity and performance when applied to electromagnetic fields. The application that we evaluated is a model of a mobile phone equipped with one ordinary transmitting antenna and a number of actuator-antennas which purpose is to cancel out the electromagnetic field at a specific volume in space (e.g. at the human head) while maintaining a predefined level of the overall output power of the system. This power control is achieved through the use of a quadratic constraint on the active control algorithm. In addition, we will also investigate the impact of MIMO antenna parameters and carrier frequency on the performance of the system. Simulation results show the promise of using the adaptive control algorithms and MIMO system to attenuate the electromagnetic field power density.

# Contents

# Chapter 1

# Introduction

There have been several studies done, with conflicting results, on the effects of cell-phone radiation on the human body [1–3]. The amount of radiation emitted from most cell phones is very minute. However, given the close proximity of the phone to the head, it is entirely possible for the radiation to cause harm. If you want to be on the safe side, the easiest way to minimize the radiation you are exposed to is to position the antenna as far from your head as possible. Utilizing a hands-free kit, a car-kit antenna or a cell phone whose antenna is even a couple of inches farther from the head can do this most effectively. This report makes a contribution to that discussion by proposing a new approach employing adaptive active control algorithms combined with a Multiple-Input Multiple-Output (MIMO) antenna system to suppress the electromagnetic field at a certain volume in space.

Active methods for attenuating acoustic pressure fields have been successfully used in many applications. In this paper we investigate if these methods can be applied to an electromagnetic field in an attempt to lower the power density at a specified volume in space.

The Cancelling out of a signal can be achieved by employing the principle of superposition. For example, if two signals are superimposed, they will add either constructively or destructively. The objective of our study is to investigate the possibility of applying adaptive active control algorithms with the goal of reducing the electromagnetic field power density at a specific volume using the superposition principle and MIMO antenna system. Initially, the application we evaluate is a model of a mobile phone equipped with one ordinary transmitting antenna and a number of actuator-antennas which purpose is to cancel out the electromagnetic field at a specific volume in space (e.g. at the human head) [4–8]using power level information obtained by an sensor antenna array. Later, we investigate the effects of the size and number of MIMO antenna elements on the performance of the system [4, 6].

It is worth stressing at this point that the purpose of this MIMO system is not to improve the capacity or quality of transmission between the mobile unit and base station, but to predict the channel response or sense the radiated field which can then be controlled by using the active control algorithms. For this purpose, a class of algorithms called Filtered-X [17,18,21], which are well known from the area of acoustic noise cancellation are employed and evaluated to assess their behaviour and performance in this electromagnetic type of environment. By constraining these adaptive algorithms we also try to make the total output power level transmitted by the antenna elements, locked to a predefined value. This power constraint is achieved through the use of a quadratic constraint on the active control algorithms [5–8].

The modelling of the antenna elements and the electromagnetic field calculations are performed using the simulation package FEMLAB (currently COMSOL Multiphysics) [9, 10]. This software is also used in combination with MATLAB to implement and test the adaptive algorithms used to control the electromagnetic field. The operating carrier frequency used in the initial investigation is 900 MHz (a wave length $\lambda$ of approximately 0.33 m). Later, we test the algorithms at different carrier frequencies (e.g., other GSM bands and UMTS) [4].

The organisation of this report is as follows. In Chapter 2, we present the FEMLAB MIMO antenna model. In Chapter 3, the different unconstrained adaptive algorithms used to suppress the power density of the electromagnetic field are presented. Simulation results comparing these different algorithms are shown in Chapter 4. The constrained solution of the output power is presented in Chapter 5. Simulation results investigating the effects of the different MIMO antenna system parameters including the operating frequency are analysed and presented in Chapter 6. Finally, Chapter 7 concludes the report and presents further research ideas.

# Chapter 2

# The Model

## 2.1 The FEMLAB model

The application used in this report is a two-dimensional (2D) cross-section model of a physical system consisting of eight vertical antenna elements and of a human head, as shown in figures 2.1 and 2.2, respectively. The simulation of the radio waves is performed numerically by using the finite element method (FEM) in FEMLAB for solving the electromagnetic field equations.

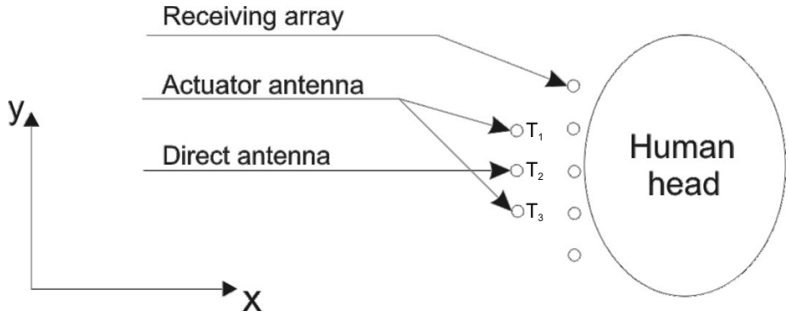


Figure 2.1: 2D model representing the tested physical system.

In a simple medium where we have no external sources except inside the transmitting antenna elements, we can write Maxwell's equations in time-harmonic form as:

$$\nabla \times \mathbf{E} = j\omega\mathbf{B} \tag{2.1}$$

$$\nabla \times \mathbf{B} = \mu\mathbf{J} - j\omega\mu\mathbf{D} \tag{2.2}$$

$$\nabla \cdot \mathbf{D} = \rho \tag{2.3}$$

$$\nabla \cdot \mathbf{B} = 0 \tag{2.4}$$

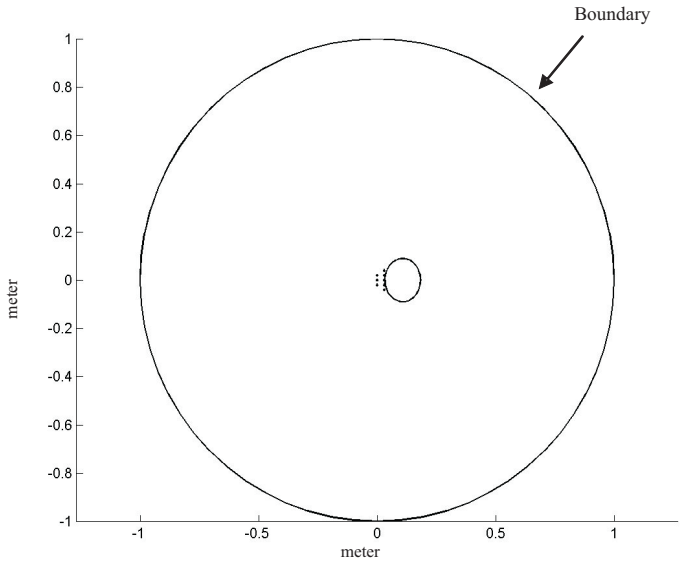


Figure 2.2: The FEMLAB representation of the 2D model in figure 2.1. The outer boundary is set to a radius of 1 meter to limit the FEM solution.

(The vector arguments and the term $e^{-j\omega t}$ are omitted for simplicity).

To solve the electric field with the current density in the antenna as the input source we eliminate the magnetic flux field $\mathbf{B}$ from equation 2.2 and get:

$$\nabla \times (\nabla \times \mathbf{E}) - \omega^2 \varepsilon \mu \mathbf{E} = j\omega\mu\mathbf{J} \tag{2.5}$$

If it is assumed that there are no free charges, then $\nabla \cdot \mathbf{E} = 0$ and we get the inhomogeneous *Helmholz's* equation:

$$\nabla^2 \mathbf{E} + \omega^2 \varepsilon \mu \mathbf{E} = -j\omega\mu\mathbf{J} \tag{2.6}$$

The parameters denoted by $\varepsilon$ (permittivity), $\mu$ (permeability)and $\sigma$ (conductivity) define the electromagnetic properties of the different materials in the model.

To model materials that contain both conductive and dielectric properties, a complex valued permittivity $\varepsilon_c$ is defined:

$$\varepsilon_c = \left( \varepsilon_r - j\frac{\sigma}{\omega\varepsilon_0} \right) \tag{2.7}$$

where $\sigma$ is the conductivity and $\varepsilon_r$ is the relative permittivity of the material when there is an incident time-harmonic wave with an angular frequency $\omega$

. The antenna elements are assumed to be made out of copper and will have the following electric properties:

$$\varepsilon_r = 1, \text{ since this is no dielectric material} \tag{2.8}$$
$$\sigma = 5.99 \cdot 10^7 [\text{S/m}] \tag{2.9}$$

To electrically model the human head is a more complicated task since it consists of organic tissues of varying electric properties. For simplicity an average of the electric properties of the brain and skull is used here; for example at a frequency of 900 MHz the following parameters are used:

$$\varepsilon_r = 45.805496 \tag{2.10}$$
$$\sigma = 0.766504 [\text{S/m}] \tag{2.11}$$

These values are based on the 4-Cole-Cole equation as described in [16]. If we assume that there are no ferromagnetic materials in this FEM model, it will be sufficient to set the permeability equal to the free space permeability $\mu = \mu_0$.

The finite element method requires that the modelled area is finite and therefore it needs an outer boundary as is clearly shown in figure 2.2. In order to simulate an electromagnetic wave travelling out towards infinity using this model, it is necessary to define the outer boundary of the modelled area so that it does not reflect any signal back towards the antennas (i.e. total absorption at the outer boundary):

$$\mathbf{n} \cdot (\mathbf{D}_{inside} - \mathbf{D}_{outside}) = 0 \tag{2.12}$$

where $\mathbf{n}$ is the normal vector of the boundary pointing outwards, and since it is a virtual boundary there are no surface charges or currents. This will then lead to a Neuman type of boundary condition:

$$\frac{\partial \mathbf{D}_z}{\partial \mathbf{n}} = -j \left(\mathbf{n} \cdot k\right) \mathbf{D}_z \tag{2.13}$$

where $k = \omega\sqrt{\varepsilon\mu}$.

In the model created here the wave will be very close to orthogonal against the boundary in all directions so there will be no significant reflection of the wave. Since $\mathbf{D} = \varepsilon\mathbf{E}$ we will get the boundary equation:

$$\mathbf{n} \cdot (\nabla \mathbf{E}_z) - \left(\omega\sqrt{\left(n_x^2 + n_y^2\right)\varepsilon\mu}\right)\mathbf{E}_z = 0 \tag{2.14}$$

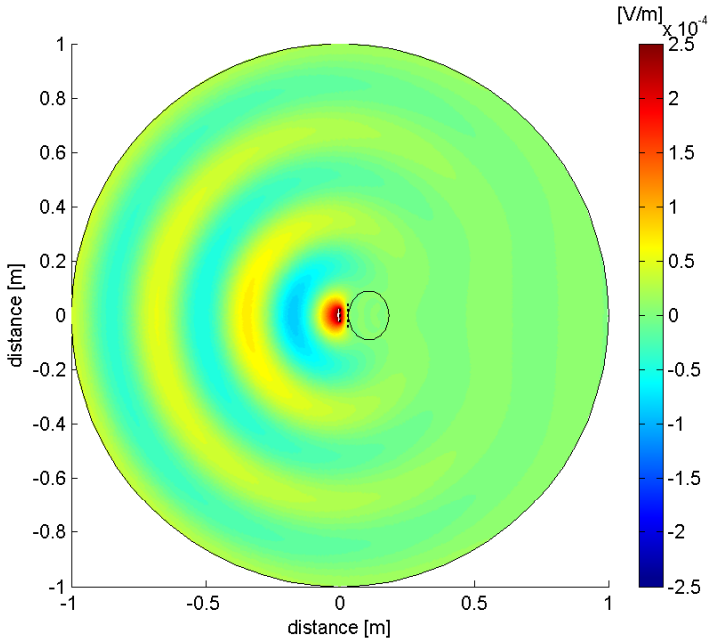


Figure 2.3: The numerical solution to the electric field problem.

When the time-harmonic solution of the electric field z-component $\mathbf{E}_z(x, y)$ is calculated (see figure 2.3), FEMLAB solves the other fields automatically using *Maxwell's equations* to get the magnetic $\mathbf{H}$, the magnetic flux density $\mathbf{B}$ and the electric displacement $\mathbf{D}$ fields, respectively.

The $\mathbf{E}_z(x, y)$ is then used to calculate the *Poynting* vector $\mathbf{S}(x, y)$ and the power density. In this case with a stationary wave, this vector can be defined as [13]:

$$\mathbf{S} = \frac{1}{\varepsilon}\mathbf{D}_z \times \frac{1}{\mu}\mathbf{B}_t = \frac{1}{\mu_0}\langle \mathbf{B}_t \cdot \mathbf{B}_t \rangle + \frac{1}{\varepsilon_0 \varepsilon_c}\langle \mathbf{D}_z \cdot \mathbf{D}_z \rangle = \frac{1}{2\mu_0}B_t^2 + \frac{1}{2\varepsilon_0 \varepsilon_c}D_z^2 \quad (2.15)$$

where $\langle \cdot \rangle$ denotes an average, subscript t denotes the tangential component and subscript z is the z component.

The best way to visualize the power density is by using a surface plot to show the magnitude of $\mathbf{S}$ in decibels as illustrated in figure 2.4.

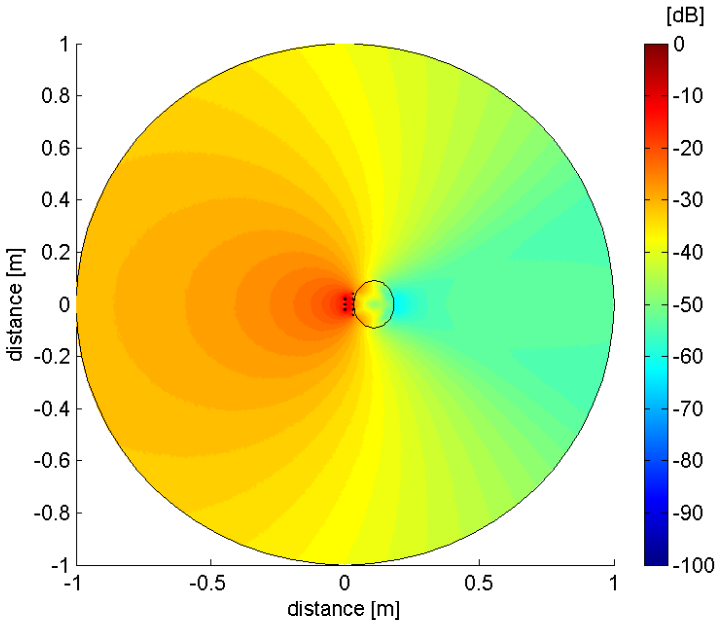


Figure 2.4: A surface plot showing the calculated magnitude of the power density based on the electric field solution.

## 2.2 The MIMO model

To reduce the electromagnetic field within a certain volume in the FEM-modelled space, a MIMO radio channel is modelled in order to compensate for the spatial displacement. In this report FEMLAB is used to simulate the physical MIMO antenna system, which (initially in this Section) consists of 3 transmitting antennas and 5 receiving antennas as shown in figure 2.1. The spacing between the antenna elements used in this application is $0.02m \ll \lambda$; thus this arrangement can not be seen as an ordinary beamformer as the antenna elements are working in the radiated near-field. The input signals to this system are three separate currents in a complex-valued phasor notation, one for each transmitting antenna. The simulated output current from the 5 receiving antennas form a complex-valued data vector denoted as the error signal vector of the system. The centre antenna $T_2$ (see figure 2.1) is transmitting the signal that we want to cancel (it acts as the antenna on any ordinary mobile telephone) and the two flank transmitter antennas $T_1$ and $T_3$ (see figure 2.1) are denoted as actuator-antennas, which will be used to reduce the signal from the antenna $T_2$ at some specified volume.

By changing the amplitudes and phases of the currents assigned to the

three transmitting antennas it is possible to control the transmitted power from the separate antenna elements. Note that since this is a two-dimensional model, there is no way to define the input voltage to the antenna in the model, and so the power output is only a relative power depending on which voltage is assumed.

The calculated time-harmonic electromagnetic wave in the model will then generate a current density inside the receiving antenna elements. According to Ampere's law for a time-harmonic wave in a simple conductive media we have the following equation:

$$\nabla \times \mathbf{B} = j\omega\mu\varepsilon_c\mathbf{E} \tag{2.16}$$

The total output current $I_{out}$ from each receiving antenna element can be calculated by integrating both sides over the cross section area $S$ of the antenna element:

$$\mathbf{I}_{out} = j\omega\varepsilon_0\left(\varepsilon_r - j\frac{\sigma}{\varepsilon_0\omega}\right)\iint_S \mathbf{E}_z \, dS \tag{2.17}$$

The result from each antenna element is then stored in a complex-valued data vector $\mathbf{e}$. If we have a system of three transmitter antennas and five receiver antennas the transmitter antenna in the middle ($T_2$) (see figure 2.1) is the one we want to cancel, then the two flanking transmitter antennas are denoted as the actuator-antennas ($T_1, T_3$).

Since the simulated model is experimentally confirmed to be linear, and this is a weak-stationary problem with a monochromatic time-harmonic signal, it is in this case sufficient to describe the parameters as a $5 \times 3$ complex-valued matrix $\mathbf{H}$:

$$\mathbf{H} = \begin{bmatrix} H_{11}(\omega) & H_{12}(\omega) & H_{13}(\omega) \\ H_{21}(\omega) & H_{22}(\omega) & H_{23}(\omega) \\ H_{31}(\omega) & H_{32}(\omega) & H_{33}(\omega) \\ H_{41}(\omega) & H_{42}(\omega) & H_{43}(\omega) \\ H_{51}(\omega) & H_{52}(\omega) & H_{53}(\omega) \end{bmatrix} \tag{2.18}$$

These complex-valued numbers $H_{ij}$ describe the amplitude and phase due to the distance between the different combinations of transmitting and receiving antennas. The general mathematical MIMO model is shown in figure 2.5

Each column in $\mathbf{H}$ represents the time-harmonic frequency response functions between one of the transmitting antennas and each of the receiving antennas. The superimposed signals received by the antenna array, constitutes a vector $\mathbf{e}$ with five complex-valued elements:

$$\mathbf{e} = \begin{bmatrix} e_1 & e_2 & e_3 & e_4 & e_5 \end{bmatrix}^T \tag{2.19}$$

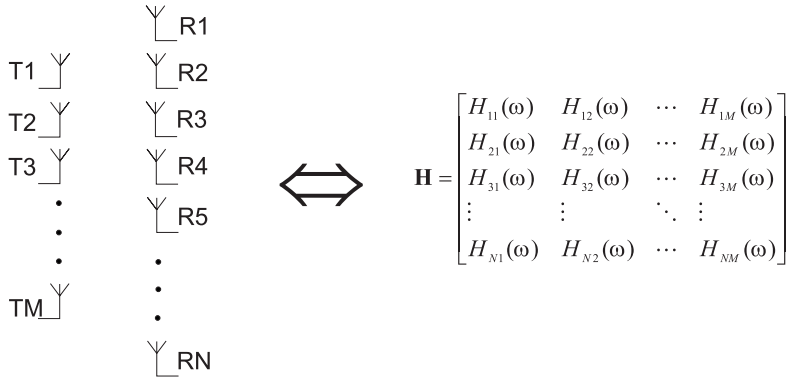


Figure 2.5: The general mathematical MIMO model of the entire antenna system.

If we divide the matrix $\mathbf{H}$ is into two separate complex-valued matrices ($\mathbf{F}$ and $\mathbf{g}$) as shown in figure 2.6, we get:

$$\mathbf{F} = [\mathbf{H}_1 \quad \mathbf{H}_3] = \begin{bmatrix} F_{11} & F_{21} & F_{31} & F_{41} & F_{51} \\ F_{12} & F_{22} & F_{32} & F_{42} & F_{52} \end{bmatrix}^T \tag{2.20}$$

and

$$\mathbf{g} = \mathbf{H}_2 = \begin{bmatrix} \mathrm{g}_1 & \mathrm{g}_2 & \mathrm{g}_3 & \mathrm{g}_4 & \mathrm{g}_5 \end{bmatrix}^T \tag{2.21}$$

The two columns in $\mathbf{F}$ represent the frequency response functions of the *actuator*-antennas and are denoted as the *forward* channels. The vector $\mathbf{g}$ is denoted as the *direct* channel and represents the frequency response function of the antenna with the signal we want to cancel out. The total noise of the model is described by vector $\mathbf{v}$, and can be modelled as a complex-valued additive white Gaussian noise vector. The vector $\mathbf{e}$ is the combined signals and noise received from the antenna array as shown in figure 2.6.

If the carrier signal transmitted through the *direct* channel $\mathbf{g}$ is to be suppressed at the receiving antenna array, a phase-shifted and amplified copy of the same carrier signal could be transmitted through the *forward* channels to superimpose the signal in the *direct* channel. This could be achieved by incorporating a filter $\mathbf{w}$ which would allow control over the signals going through the *forward* channels as shown in figure 2.7.

To achieve the best possible attenuation in energy sense, the total energy output $\xi$ of the signal $\mathbf{e}$ at the receiving antennas must be as low as possible. The minimum energy with respect to the filter $\mathbf{w}$ is:

$$\min_{\mathbf{w}} \ \xi = \min_{\mathbf{w}} \mathrm{E}\{|\mathbf{e}|^2\} = \min_{\mathbf{w}} \mathrm{E}\{\mathbf{e}^H\mathbf{e}\} \tag{2.22}$$

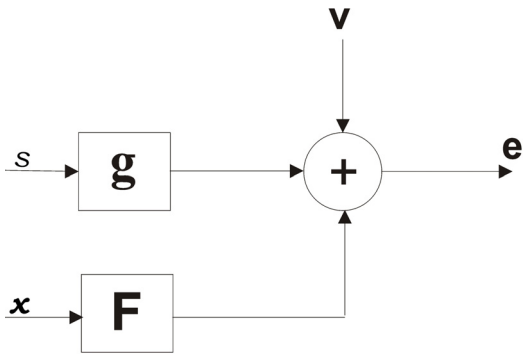


Figure 2.6: Block diagram of the antenna system described as two channels.

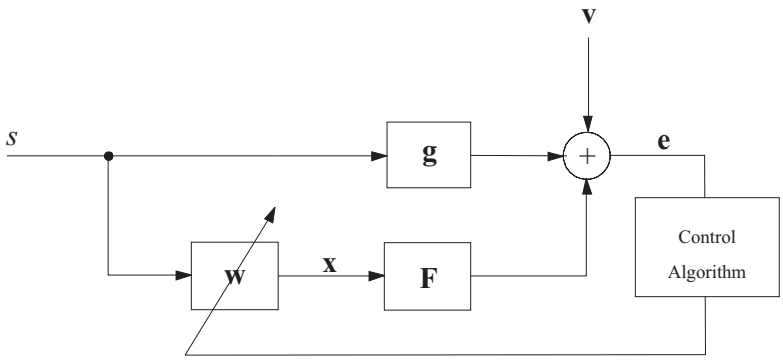


Figure 2.7: Model of the *direct* channel **g**, and the *forward* channels **F** controlled by the filter **w**.

where H denotes a conjugate transpose. With the noise **v** included in the system, the residual error signal **e** in equation 2.19 is given by:

$$\mathbf{e} = s\mathbf{g} + s\mathbf{F}\mathbf{w} + \mathbf{v} \tag{2.23}$$

If the input signal $s$ and the noise **v** are assumed to be uncorrelated, then the mean energy can be written as:

$$\xi = \mathrm{r}_d + \mathbf{w}^H\mathbf{p} + \mathbf{p}^H\mathbf{w} + \mathbf{w}^H\mathbf{R}_F\mathbf{w} + \mathrm{r}_v \tag{2.24}$$

where $\mathbf{R}_F$ is the covariance matrix of the *forward* channels, **p** is the cross-correlation between the *direct* channel and the *forward* channels, $\mathrm{r}_d$ and $\mathrm{r}_v$ are the signal power of the *direct* channel and the noise, respectively.

The minimum energy $\xi_{min}$ is found by differentiating $\xi$ with respect to the complex conjugate of filter coefficients $\mathbf{w}^*$ and then setting the derivative

equal to zero:

$$\nabla_{\mathbf{w}^*}\xi = 0 \quad \Leftrightarrow \quad \mathbf{p} + \mathbf{R}_F\mathbf{w} = 0 \tag{2.25}$$

$$\mathbf{w}_{opt} = -\mathbf{R}_F^{-1}\mathbf{p} \tag{2.26}$$

This is the *Least Mean Square* (LMS) solution to the problem and is the optimal solution in mean energy sense. Figure 2.9 shows the surface plot of the power density solution when the filter coefficients controlling the signals going through the forward channels are the optimal least mean square coefficients $\mathbf{w}_{opt}$ obtained from equation 2.26.

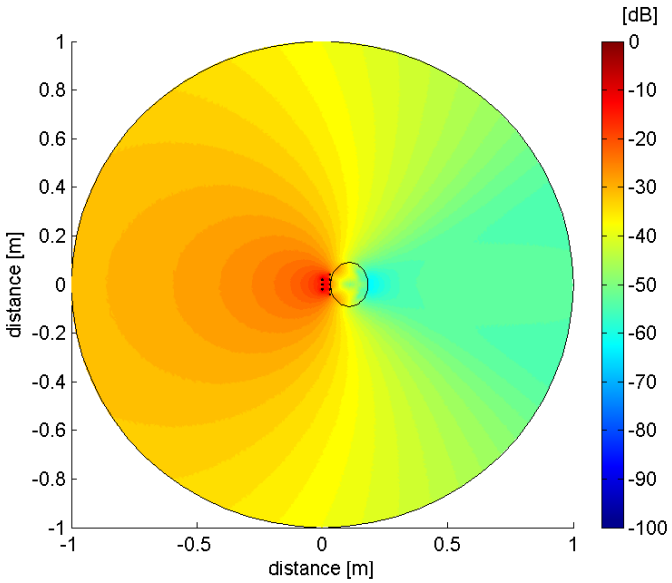


Figure 2.8: The power density in the model when there i no optimization.

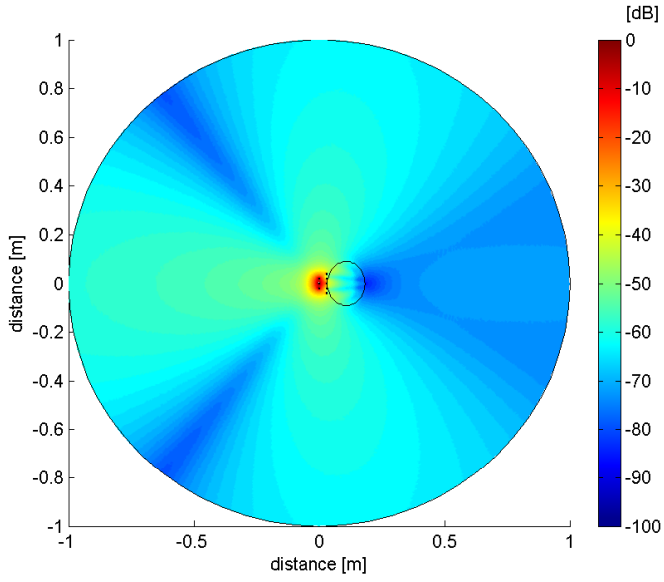


Figure 2.9: The power density in the model when the optimal filter coefficients $\mathbf{w}_{opt}$ are used.

# Chapter 3

# The Adaptive Algorithms

The least mean square solution in equation 2.24 describes a quadratic form in the complex valued **w**-domain, and there is only one optimum point. The gradient of the quadratic performance surface will be evaluated with respect to the conjugate filter coefficients: $-\nabla_{\mathbf{w}^*}\xi$ . This will give the local steepest descent direction towards the minimum point of the performance surface. To give some idea of how these complex valued filter coefficients move toward the minimum point, the magnitude of the filter coefficients are plotted in figure 3.1 and in figures 3.2-3.5 and figure 5.1 for the other different adaptive algorithms.

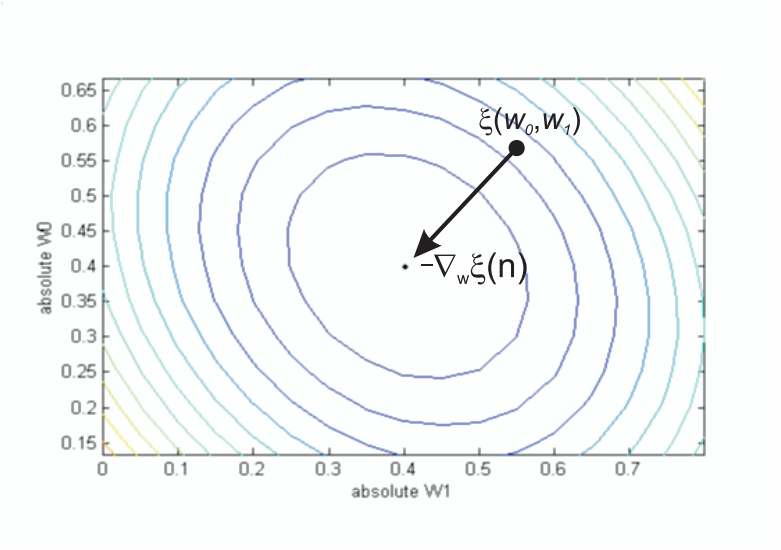


Figure 3.1: The quadratic performance surface where the energy $\xi$ is depicted as equivalued closed contour-curves.

If the point $(w_0, w_1)$ in figure 3.1 has the energy value $\xi$, then a new point in direction of the negative gradient vector must be closer to the minimum point of the surface. So this will give an iterative update equation of the filter-coefficients as:

$$\mathbf{w}_{\mathrm{n}+1} = \mathbf{w}_{\mathrm{n}} + (-\nabla_{\mathbf{w}^*}\xi(n)) \tag{3.1}$$

The mean-energy $\xi$ of the error function can according to equations 2.22 and 2.23 be expressed as:

$$\begin{aligned}\xi = \mathrm{E}\left\{|\mathbf{e}|^2\right\} = \mathrm{E}\left\{\mathbf{e}^H\mathbf{e}\right\} = \\ \mathrm{E}\Big\{\left(s\mathbf{g} + s\mathbf{F}\mathbf{w} + \mathbf{v}\right)^H\mathbf{e}\Big\}\end{aligned} \tag{3.2}$$

If we differentiate equation 3.2 with respect to the conjugate of the filter coefficients $\mathbf{w}^*$ we get the gradient of the mean energy:

$$-\nabla_{\mathbf{w}^*}\xi = -\mathrm{E}\left\{\mathbf{F}^H s^*\mathbf{e}\right\} \tag{3.3}$$

Define $\mathbf{F}^H s^* \equiv \mathbf{X}^H$, we get:

$$-\nabla_{\mathbf{w}^*}\xi = \mathrm{E}\left\{-\mathbf{X}^H\mathbf{e}\right\} \tag{3.4}$$

The expected value is generally unknown, so this can be estimated by a sample mean instead; that is:

$$-\hat{\nabla}_{\mathbf{w}^*}\xi = -\mathbf{X}^H\mathbf{e} \tag{3.5}$$

where $\hat{\nabla}$ denotes the estimated gradient.

If this is substituted into the weight-updating equation 3.1 we get:

$$\mathbf{w}_{\mathrm{n}+1} = \mathbf{w}_{\mathrm{n}} + \mu\left(\nabla_{\mathbf{w}^*}\xi(n)\right) = \mathbf{w}_{\mathrm{n}} - \mu\mathbf{X}^H\mathbf{e} \tag{3.6}$$

This is the so-called Filtered-X LMS [17, 21] (FX-LMS), since $\mathbf{X}$ is the input signal filtered through the *forward* channels $\mathbf{F}$. The step-length $\mu$ in FX-LMS is a constant value and therefore the stability range and convergence rate will change with the change of input power as:

$$0 < \mu < \frac{2}{\mathrm{tr}\left(\mathbf{R}_F\right)} \tag{3.7}$$

To get around the change of convergence rate, consider that:

$$\mathbf{R}_F = s^*\mathbf{F}^H\mathbf{F}s = |s|^2 \cdot \begin{bmatrix} \sum_{m=1}^{5}|F_{m1}|^2 & \sum_{m=1}^{5}F_{m1}^*F_{m2} \\ \sum_{m=1}^{5}F_{m1}F_{m2}^* & \sum_{m=1}^{5}|F_{m2}|^2 \end{bmatrix} \tag{3.8}$$

Then the trace of the matrix $\mathbf{R}_F$ will be:

$$\mathrm{tr}\left(\mathbf{R}_F\right) = |s|^2 \sum_{m=1}^{5} |F_{m2}|^2 |F_{m1}|^2 \tag{3.9}$$

where $m$ designates the five different receiving antennas. The above range for convergence (equation 3.7) can then be written as:

$$0 < \mu < \frac{2}{|s|^2 \sum_{m=1}^{5} |F_{m2}|^2 |F_{m1}|^2} \tag{3.10}$$

If we introduce a new step-length parameter $\beta\,(0 < \beta < 2)$ and normalize by the trace of the matrix $\mathbf{R}_F$ , we get:

$$\mu = \frac{\beta}{|s|^2 \sum_{m=1}^{5} |F_{m2}|^2 |F_{m1}|^2} \tag{3.11}$$

Then the range of the step-length will be fixed within the range $0 < \beta < 2$. If this substitution is made in the FX-LMS weight-updating algorithm (equation 3.6), we get the Normalized FX-LMS algorithm:

$$\mathbf{w}_{\mathrm{n}+1} = \mathbf{w}_{\mathrm{n}} + \beta \left( \frac{\mathbf{X}_n^H}{\alpha + \mathrm{tr}\left(\mathbf{R}_F\right)} \right) \mathbf{e} \tag{3.12}$$

where $\alpha$ is a noise regulating parameter if the elements of $\mathbf{R}_F$ are small [17, 21].

Another approach to an adaptive algorithm is by using the optimal least mean square solution from equation 2.26 in combination with the gradient vector of the quadratic performance surface [17, 21]:

$$\nabla\xi = \mathbf{R}_F\mathbf{w} + \mathbf{p} \tag{3.13}$$

If we multiply both sides of the gradient by $\mathbf{R}_F^{-1}$, we get:

$$\mathbf{R}_F^{-1}\nabla\xi = \mathbf{w} - \mathbf{w}_{opt} \tag{3.14}$$

Rearrange equation 3.14 into an iterative equation where $\mathbf{w}_{\mathrm{n}} = \mathbf{w}$ is the present position (or iteration) and $\mathbf{w}_{\mathrm{n}+1} = \mathbf{w}_{opt}$ is the next position, we get:

$$\mathbf{w}_{\mathrm{n}+1} = \mathbf{w}_{\mathrm{n}} - \mathbf{R}_F^{-1}\nabla_{\mathrm{n}}\xi \tag{3.15}$$

If the expression of the gradient vector is inserted into equation 3.15 we obtain:

$$\mathbf{w}_{\mathrm{n}+1} = \mathbf{w}_{\mathrm{n}} - \mathbf{R}_F^{-1}\left(\mathbf{R}_F\mathbf{w}_{\mathrm{n}} + \mathbf{p}\right) = \mathbf{w}_{opt} \tag{3.16}$$

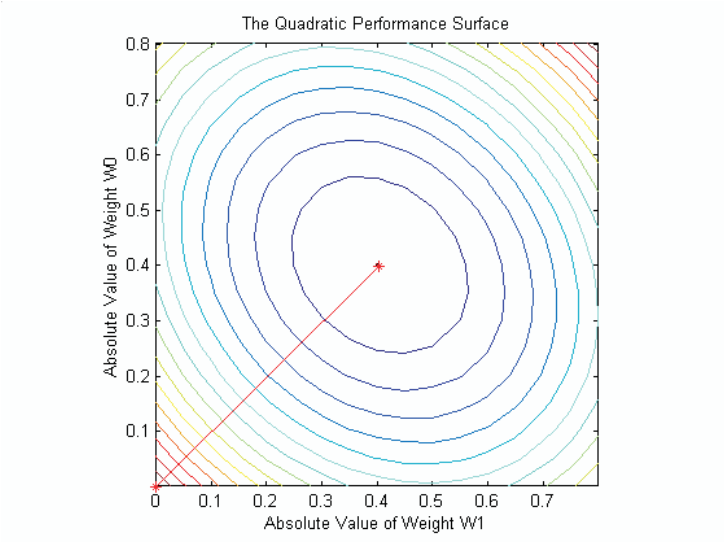


Figure 3.2: The Newton algorithm finds the minimum point in one step. SNR = 30 dB.

This is the FX-Newton algorithm and its iterative equation moves from any arbitrary point $\mathbf{w}_{\mathrm{n}}$ on the performance surface to the minimum point in one single step. This can be clearly seen in figure 3.2 for a signal-to-noise ratio (SNR) of 30 dB.

If the noise level is high (i.e., low SNR), this can give a very erratic search of the minimum point with a large misadjustment (i.e. noise) as illustrated in figure 3.3.

One approach to smooth the misadjustment noise is by using a step-length variable $\mu$ as a smoothing regulator:

$$\mathbf{w}_{\mathrm{n}+1} = \mathbf{w}_{\mathrm{n}} - \mu \mathbf{R}_F^{-1} \left( \mathbf{R}_F \mathbf{w}_{\mathrm{n}} + \mathbf{p} \right) \tag{3.17}$$

where $0 < \mu < 1$.

This solution is still going to give an erratic search with a large misadjustment, unless a very small step-length is used which will also slow down the rate of convergence. However, if the gradient vector $(\mathbf{R}_F \mathbf{w}_{\mathrm{n}} + \mathbf{p})$ is estimated by the sample mean as was done in the FX-LMS algorithm [17], we get:

$$-\hat{\nabla}_{\mathbf{w}^*} \xi = \hat{E} \left\{ \mathbf{X}^H \mathbf{e} \right\} = \mathbf{X}^H \mathbf{e} \tag{3.18}$$

where *denotesanestimation*.

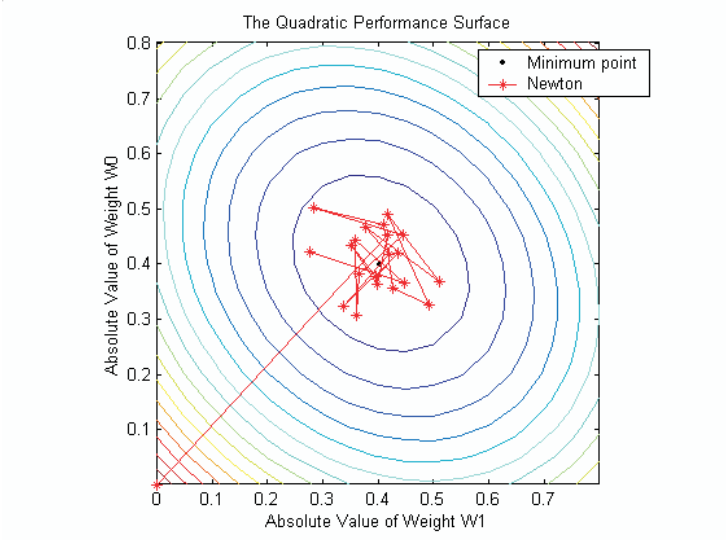


Figure 3.3: The erratic search of the Newton algorithm when the noise level is high. SNR = 10 dB.

Using equation 3.18, the new weight update equation is given by:

$$\mathbf{w}_{\mathrm{n}+1} = \mathbf{w}_{\mathrm{n}} - \mu \mathbf{R}_F^{-1} \left( \hat{\nabla}_{\mathbf{w}_{\mathrm{n}}^H} \xi \left( n \right) \right) = \mathbf{w}_{\mathrm{n}} - \mu \mathbf{R}_F^{-1} \mathbf{X}_{\mathrm{n}}^H \mathbf{e} \tag{3.19}$$

This is the so-called FX-Newton/LMS algorithm, which is a compromise between the two adaptive approaches. This will result in a greatly enhanced smoothing of the gradient-noise as can be seen from figure 3.4.

The main problem with both the FX-Newton and the FX-Newton/LMS algorithms is the need to calculate the inverse of the covariance matrix, which is computationally inefficient. However, if the diagonal elements of the covariance matrix $\mathbf{R}_F$ are large compared to the off-diagonal values, then the covariance matrix can be estimated from:

$$\hat{\mathbf{R}}_F \approx diag \left\{ \mathbf{R}_F \right\} \tag{3.20}$$

By inserting this estimate into the weight updating equation and using a separate step-length for each matrix element, we get:

$$\mathbf{w}_{\mathrm{n}+1} = \mathbf{w}_{\mathrm{n}} - \mathbf{M} \mathbf{X}_{\mathrm{n}}^H \mathbf{e} \tag{3.21}$$

where

$$\mathbf{M} = \begin{bmatrix} \frac{\mu_1}{|s|^2 \cdot \sum_{m=1}^{5} |F_{m1}|^2} & 0 \\ 0 & \frac{\mu_2}{|s|^2 \cdot \sum_{m=1}^{5} |F_{m2}|^2} \end{bmatrix}$$

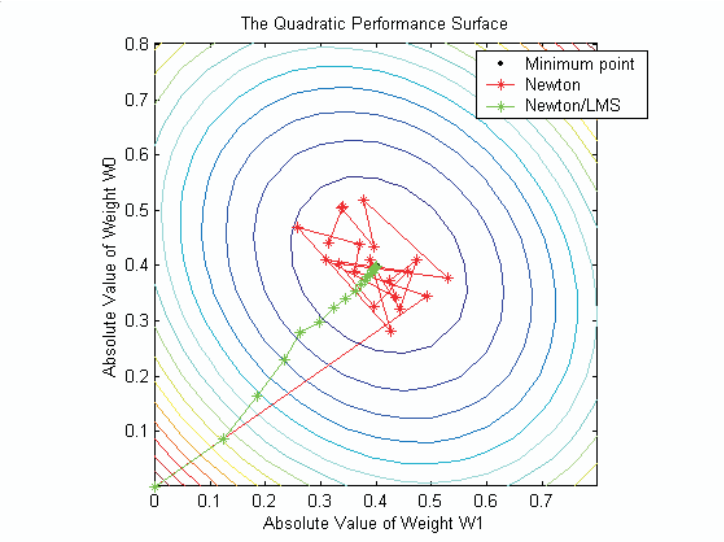


Figure 3.4: This plot clearly shows why the Newton/LMS algorithm (the green trace) is preferable to the ordinary relaxed Newton algorithm (the red trace) when a high noise level is present in the estimation of the gradient vector. SNR = 10 dB.

Equation 3.21 is known as the Actuator Individual Normalized FX-LMS algorithm [18].

If the eigenvalues of $\mathbf{R}_F$ are disparate, then the Actuator Individual Normalized FX-LMS will outperform the Normalized FX-LMS since each filter weight will be controlled and normalized separately. On the other hand, if the eigenvalues of the covariance matrix roughly have the same value, then the Normalized FX-LMS and the Actuator Individual Normalized FX-LMS behave in a similar way as can be seen from figure 3.5.

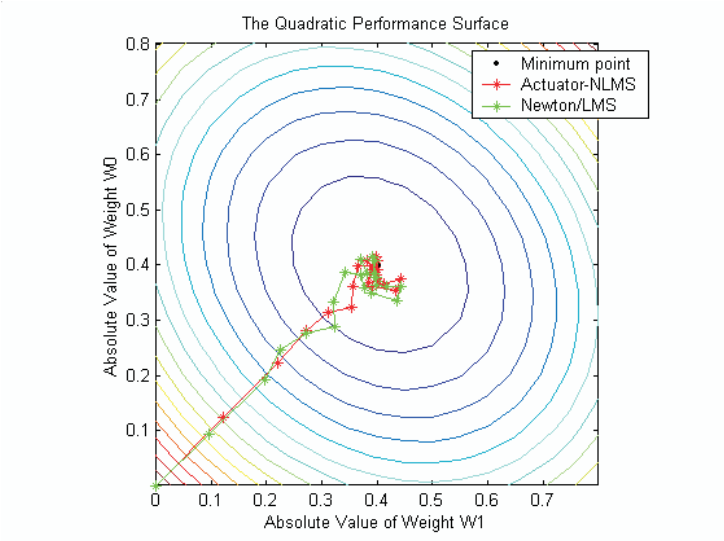


Figure 3.5: This show the comparison between the Actuator Individual Normalized FX-LMS and the FX-Newton/LMS. Since the eigenvalues of $\mathbf{R}_F$ and of diag $(\mathbf{R}_F)$ are roughly the same the two algorithms will behave in a similar fashion.

# Chapter 4

# Simulation Results

In the previous section we presented the different adaptive algorithms to suppress the power density of the electromagnetic field. These algorithms are unconstrained; that is there is no control over the total output power from the mobile phone. In chapter 5, the constrained solution will be presented. In this section we evaluate and compare the different unconstrained adaptive algorithms.

The ordinary FX-LMS algorithm is the simplest to implement of the evaluated algorithms, but this algorithm has some disadvantages when the input signal is non-stationary. The Normalized FX-LMS algorithm normalizes the input signal with its signal power, resulting in a more robust algorithm at the expense of higher computational complexity. Another approach to the adaptive search is Newton's method where it is possible to solve the problem in one single step under ideal conditions. This single-step algorithm, however, is very sensitive to noise and is therefore impractical. To improve the noise insensitivity of the Newton algorithm, a gradient vector estimate is used to smooth the algorithm. This algorithm is called the FX-Newton/LMS. Both the FX-Newton and FX-Newton/LMS algorithms require a matrix inversion of the covariance matrix, resulting in high computational complexity. The Actuator Individual Normalized FX-LMS algorithm only uses the diagonal of the covariance matrix to simplify the problem of calculating the inverse of the covariance matrix.

From the above discussion and by testing the algorithms by simulations, it was concluded that the Normalized FX-LMS and the Actuator Individual Normalized FX-LMS are the preferred algorithms since they are both robust and noise-insensitive. Figure 4.1 shows the calculated average power level inside the human head relative to the power level of a single transmitting antenna for both adaptive algorithms. The figure also show the corresponding power level attained by employing a passive five element reflector and the

least mean square solution which is used as a benchmark for comparisons.

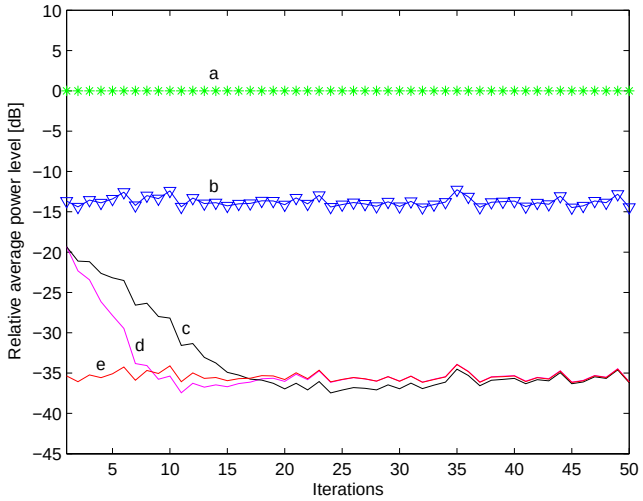


Figure 4.1: The relative average power level inside the human head. Plots (from top to bottom):
a) One transmitting antenna only.
b) 5 passive sensor elements as a passive reflector.
c) FX-LMS.
d) Actuator Individual FX-NLMS.
e) Least Mean Square solution.

The amount of attenuation achieved by the least mean square solution is approximately 36 dB relative to the power level produced by a single antenna system (i.e., by using the direct transmitting antenna only, as shown in figure 2.1). It is clear from figure 4.1 that the adaptive algorithms after convergence give about 23 dB more attenuation compared to using the five receiving antenna elements as a passive reflector. It can also be seen that the Actuator Individual FX-NLMS converges about 40% faster than the FX-NLMS towards the least mean square solution, since each diagonal element of the covariance matrix is normalized separately.

Finally, in figure 4.2 we show the power density field for one transmitting antenna with five passive reflector elements, and in in figure 4.3 three transmitting antennas tuned to the least mean square solution (i.e., the adaptive algorithms after convergence), respectively. It is clearly evident from this surface plot that the electromagnetic power density field inside the head is lower in the adaptive algorithms case.

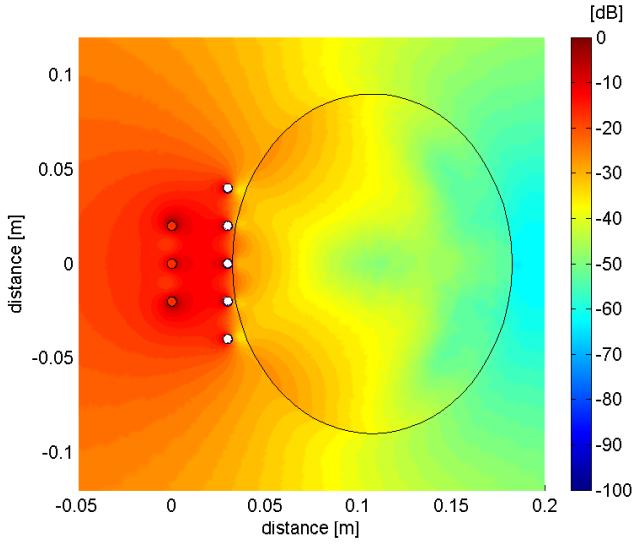


Figure 4.2: Power density surface plot inside the human head (referring to figure 2.1) using one active transmitting antenna with five passive reflector elements (plot b in figure 4.1)

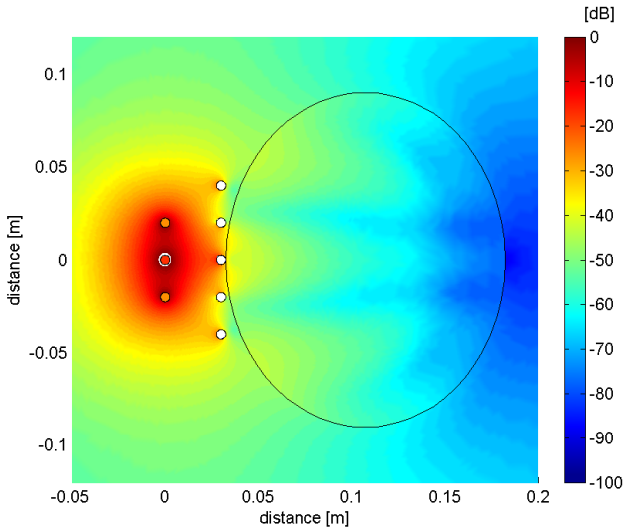


Figure 4.3: Power density surface plot inside the human head (referring to figure 2.1) using three transmitting antennas tuned to the least mean square solution (plot e in 4.1)

# Chapter 5

# Power Constraints

In the previous sections we presented the different unconstrained adaptive algorithms to suppress the power density of the electromagnetic field and their respective simulation results. There is however a major drawback with these adaptive algorithms: that is although the field is attenuated by approximately 15 dB (as shown in plots c-e in figure 4.1) inside the human head, there is no control over the total output power from the mobile phone. This means that the total output power changes when the filter adapts, which is unfortunate since the magnitude of the total output power from the mobile phone depends on the distance from the base station. For example, if we take the case of three transmitting antennas and five receiving antennas, this would result in an increase of the total output power by approximately 20% (although this still gives a suppression of 15 dB inside the human head). However, with some other antenna spacing the mobile phone might lose the connection when the adaptive suppression filter converges towards the optimum value.

To alleviate this problem, some form of power constraint [5] could be used on the minimization process; that is:

$$\begin{aligned} &\min_{\mathbf{w}^H} \left( \mathrm{r}_d + \mathbf{w}^H\mathbf{p} + \mathbf{p}^H\mathbf{w} + \mathbf{w}^H\mathbf{R}_F\mathbf{w} + \mathrm{r}_v \right) \\ &\text{subject to: } |s\mathbf{w}|^2 + |s|^2 = C, \quad C \in \Re \end{aligned} \tag{5.1}$$

where the symbol $\Re$ denotes a real number. This optimization problem can then be solved by forming a Lagrange equation [22] defined as:

$$\mathcal{L}(\mathbf{w}, \lambda) = \mathbf{w}^H\mathbf{R}_F\mathbf{w} + \mathbf{w}^H\mathbf{p} + \mathbf{p}^H\mathbf{w} - \lambda\left(C - s^*\mathbf{w}^H\mathbf{w}s - s^*s\right) \tag{5.2}$$

By differentiating this Lagrange equation and setting it to zero, we get a suboptimal solution of $\mathbf{w}$ which is dependent on the variable $\lambda$:

$$\nabla_{\mathbf{w}^H}\mathcal{L}(\mathbf{w}, \lambda) = 0 \quad \Leftrightarrow \quad \mathbf{R}_F\mathbf{w}_{co} + \mathbf{p} + \lambda|s|^2\mathbf{w}_{co} = 0 \tag{5.3}$$

$$\left(\mathbf{R}_F + \lambda \left|s\right|^2 \mathbf{I}\right) \mathbf{w}_{co} = -\mathbf{p} \tag{5.4}$$

where $\mathbf{w}_{co}$ denote the *constrained* values of the filter coefficients. If we multiply equation 5.4 by $\mathbf{R}_F^{-1}$ we get:

$$\left(\mathbf{I} + \lambda \left|s\right|^2 \mathbf{R}_F^{-1}\right) \mathbf{w}_{co} = -\mathbf{R}_F^{-1}\mathbf{p} \tag{5.5}$$

The right hand side of equation 5.5 is the unconstrained optimal solution $\mathbf{w}_{opt}$ which was derived earlier in this report (see equation 2.26). Using this information and rearranging equation 5.5, we get:

$$\mathbf{w}_{co} = -\left(\mathbf{I} + \lambda \left|s\right|^2 \mathbf{R}_F^{-1}\right)^{-1} \mathbf{w}_{opt} \tag{5.6}$$

It can be clearly seen from equation 5.6 that it is now possible to adjust the unconstrained solution by using a diagonal loading of the covariance matrix. The parameter $\lambda$ can be chosen so that equation 5.6 satisfies the constraint. Unfortunately there are no closed form solutions for the optimal value of the loading variable $\lambda$. However, equation 5.6 can be simplified by employing a Maclaurin expansion of the first term on the right hand side, for values of $\lambda$ that are close to zero. If we use the first two terms of the *MacLaurin* expansion (see equation 5.7), it is possible to derive an approximate expression where we only need to perform a single matrix inversion operation:

$$\left(\mathbf{I} + \lambda \left|s\right|^2 \mathbf{R}_F^{-1}\right)^{-1} \approx \mathbf{I} - \lambda \left|s\right|^2 \mathbf{R}_F^{-1} \tag{5.7}$$

When this approximation is substituted into the solution of the constrained minimization, we get the constrained values of the filter coefficients as:

$$\mathbf{w}_{co} = -\mathbf{w}_{opt} - \lambda \left|s\right|^2 \mathbf{R}_F^{-1}\mathbf{w}_{opt} \tag{5.8}$$

To find out which value of $\lambda$ we need, the constraint (equation 5.9) should be solved for the value of the constrained filter coefficients $\mathbf{w}_{co}$ and the required power constraint level C:

$$\left|s\mathbf{w}_{co}\right|^2 + \left|s\right|^2 = C \tag{5.9}$$

This will yield a quadratic equation which has the following solution:

$$\lambda = \frac{-2 \cdot \Re\left\{\mathbf{w}_{opt}^H \mathbf{q}\right\} \pm \sqrt{\left(2 \cdot \Re\left\{\mathbf{w}_{opt}^H \mathbf{q}\right\}\right)^2 - 4 \cdot \mathbf{q}^H\mathbf{q}\left(\mathbf{w}_{opt}^H\mathbf{w}_{opt} + 1 - \frac{C}{\left|s\right|^2}\right)}}{2 \cdot \left|s\right|^2 \mathbf{q}^H\mathbf{q}} \tag{5.10}$$

$$\text{where} \quad \mathbf{q} = \mathbf{R}_F^{-1}\mathbf{w}_{opt}.$$

So, by setting the constraining power level C and using the unconstrained optimal values of the filter coefficients $\mathbf{w}_{opt}$, we can now use equation 5.10 to calculate what the value of $\lambda$ should be. This value is then inserted into equation 5.8 in order to calculate the constrained filter coefficients $\mathbf{w}_{co}$, which (for convenience) is re-stated again here:

$$\mathbf{w}_{co} = -\mathbf{w}_{opt} - \lambda \left|s\right|^2 \mathbf{R}_F^{-1} \mathbf{w}_{opt} \tag{5.11}$$

As an example, if the constrained filter coefficients of equation 5.11 are used in the iterative FX-LMS adaptive algorithms, it can be seen in figure 5.1 that it will converge at the non-optimal solution that satisfy the constraint and has the shortest distance to the unconstrained optimal point. The convergence of this non-optimal constrained least square solution for the Actuator Individual FX-NLMS can also be observed in figure 5.2 and in figure 5.3 is shown the power density inside the human head when the Actuator Individual FX-NLMS algorithm have reached the constrained least square solution.

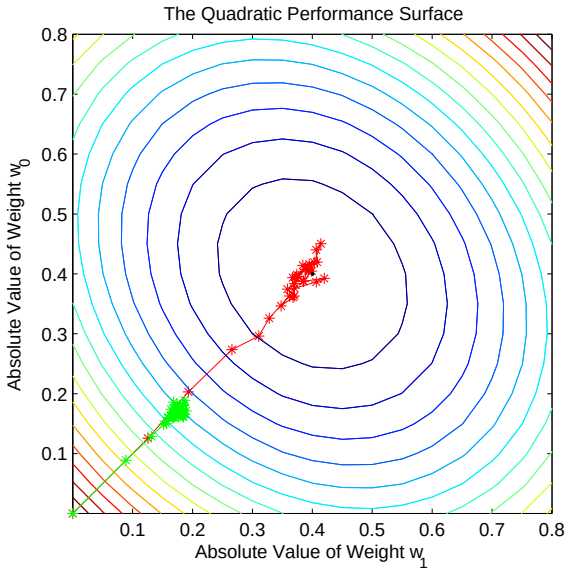


Figure 5.1: An example of using the power constraint in combination with the FX-LMS algorithm. The red trace shows the convergence of the unconstrained filter coefficients. In the green trace we have a constraint that allows for half the power needed to reach the optimal point.

In figure 5.3 and figure 5.4 we show the effect of using an adaptive algorithm with a power constraint imposed on the solution. The purpose of

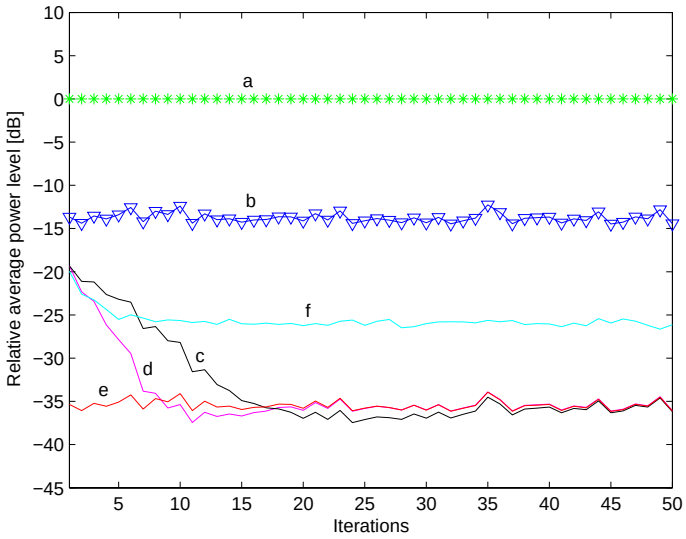


Figure 5.2: The relative average power level inside the human head. Plots (from top to bottom):
a) One transmitting antenna only.
b) 5 passive sensor elements as a passive reflector.
c) FX-LMS.
d) Actuator Individual FX-NLMS.
e) Least Mean Square solution.
f) Actuator Individual FX-NLMS with constraint.

this constraint is to allow for maximum attenuation inside the human head while keeping the radiated power from the antenna system at a level consistent with the specified radiated output power from a mobile phone. The adaptive algorithm used in figure 5.3 and figure 5.4 as well as in figure 5.2 is the Actuator Individual Normalized FX-LMS algorithm with an imposed constraint according to equation 5.11.

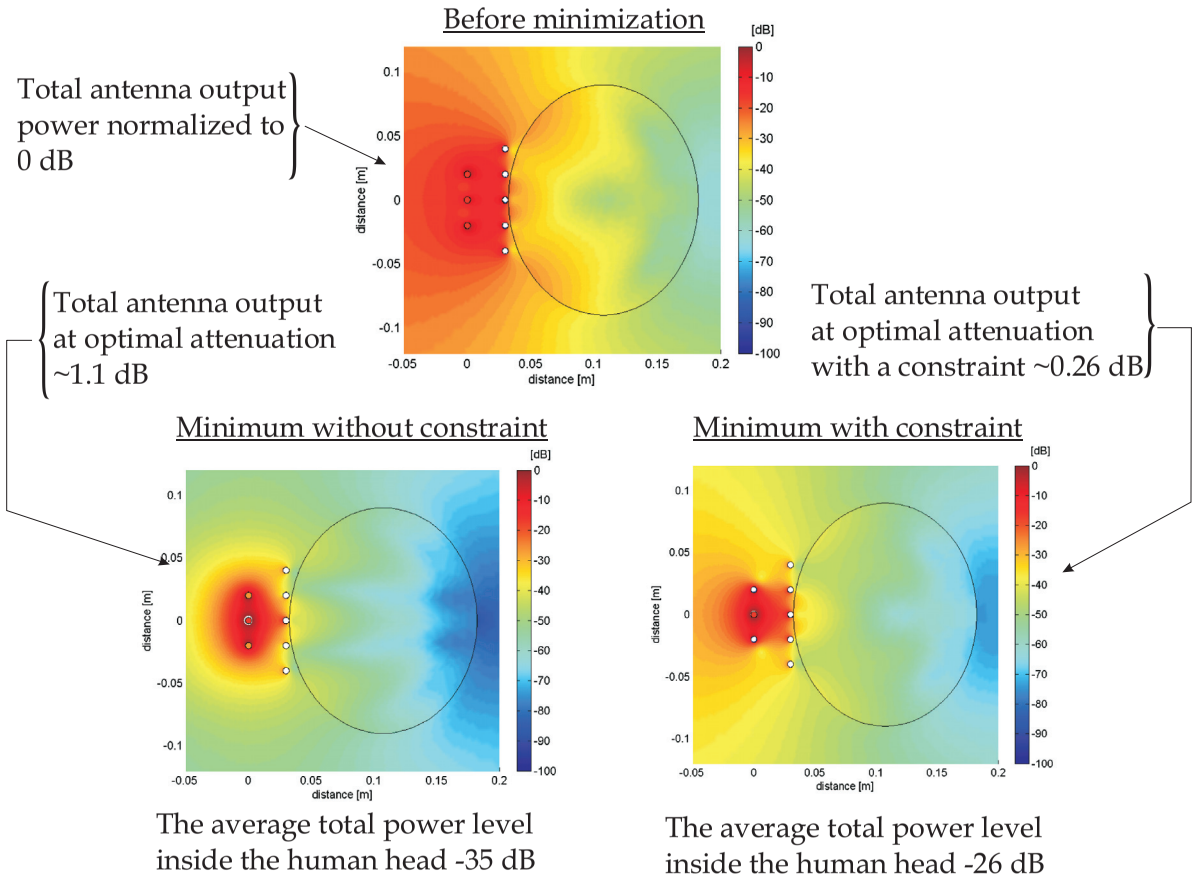


Figure 5.3: Power density suface plots inside the human head. Comparing the attenuation of electromagntic energy inside the human head and the radiated power from the antenna system without constraint (bottom left figure) and with a constraint (bottom right figure). All three figures have the distance in $x$ and $y$ directions measured in meters.

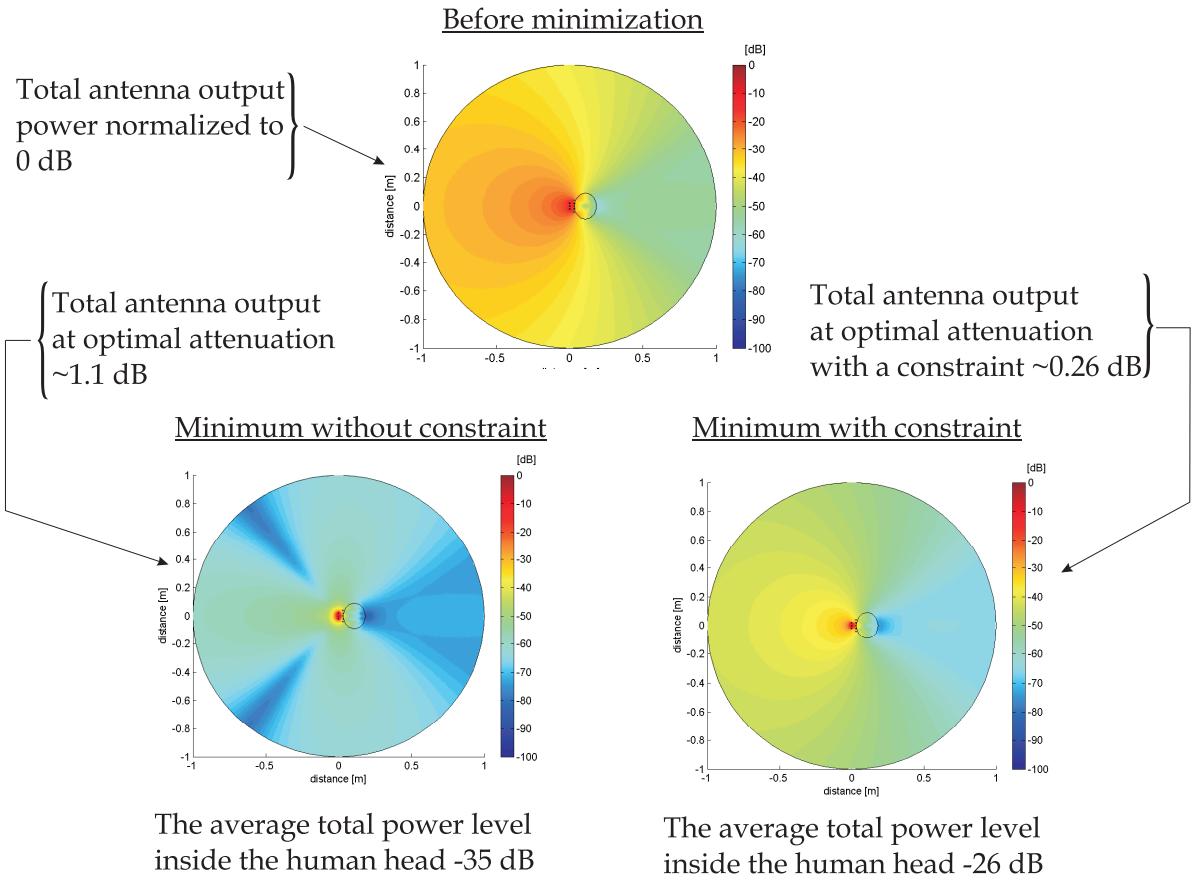


Figure 5.4: The same results as in figure 5.3, but the three plots are zoomed out to show more of the far-field. Comparing the attenuation of electromagntic energy inside the human head and the radiated power from the antenna system without constraint (bottom left figure) and with a constraint (bottom right figure). All three figures have the distance in $x$ and $y$ directions measured in meters.

# Chapter 6

# The Effects of MIMO Antenna Parameters and Carrier Frequency

The Least Mean Square solution obtained in chapter 4 is the optimal solution in energy sense for this problem. This particular solution (2.4) is only valid assuming the position of each element does not change. However, there might be positions of the antenna elements that are more favorable with respect to the power density inside the head. By changing the spacing of the antenna elements during calculations of the attenuated power level inside the human head we will investigate if there exist some optimal spacing between the different antenna elements.

In this FEMLAB model setup we assume three degrees of freedom (DOF), as shown in figure 6.1. The spacing between the sensor elements, denoted $\Delta$y, the distance (d) between the sensor element array (the receiving elements) and the actuator element array (the transmitting elements). The third DOF is the spacing between the actuator elements, denoted $\Delta$a. In the first analysis we look at how the spacing of the sensor elements and the distance between the transmitter and receiver antennas affect the power level inside the head, see figure 6.2.

It is clear from figure 6.2 that the farther apart the transmitter and receiver antennas are located the lower the power level is inside the head. This is due to the increase of the distance (d) (see figure 6.1) between the transmitter and receiver antennas. An increase of this distance will also increase the distance between the transmitter antennas and the head which will decrease the power level inside the head. By analyzing figure 6.2 we can see that the two-dimensional cost function $J(\Delta y, d)$ is flattening out at a distance d of approximately 25 cm. The spacing between the sensor elements

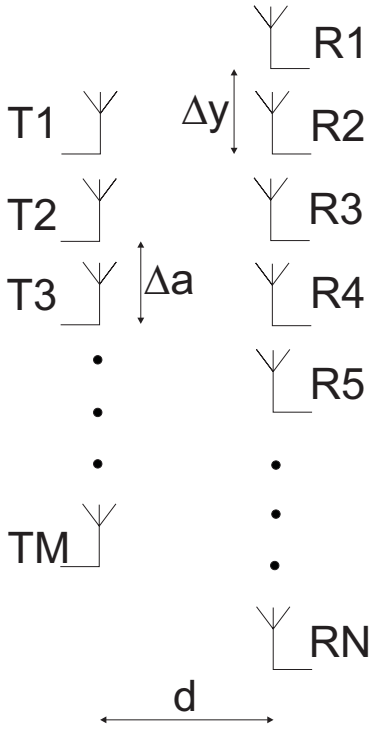


Figure 6.1: The MIMO system showing the three variables of the antenna displacement.

(receiving elements) at the distance d=25 cm should be approximately 5 cm. With this spacing the sensor element array will cover a larger portion of the head. By using these values as a good approximation of the optimal displacement of the actuator elements and the distance between the sensor elements this would result in an attenuation of approximately 50-55 dB's. Using these values as a starting point, figure 6.3 is showing how the separation of the actuator antenna elements $\Delta a$ affects the power level of the cost function $J(\Delta y, d)$ inside the head.

From figure 6.3 we can see that the attenuation inside the head will increase as the spacing between the actuator elements decrease. This is a consequence of the electromagnetic waves being transmitted from almost the same point in space. The theoretical extreme of this is to place all actuator antennas in the exact same position, which will give a complete cancellation of the waves and would give a zero power level inside the head. According to this analysis we need a MIMO antenna system that has a spacing of 5 cm between the sensor elements and a spacing of 3 cm between the actuator elements. The distance between the sensor elements and actuator elements

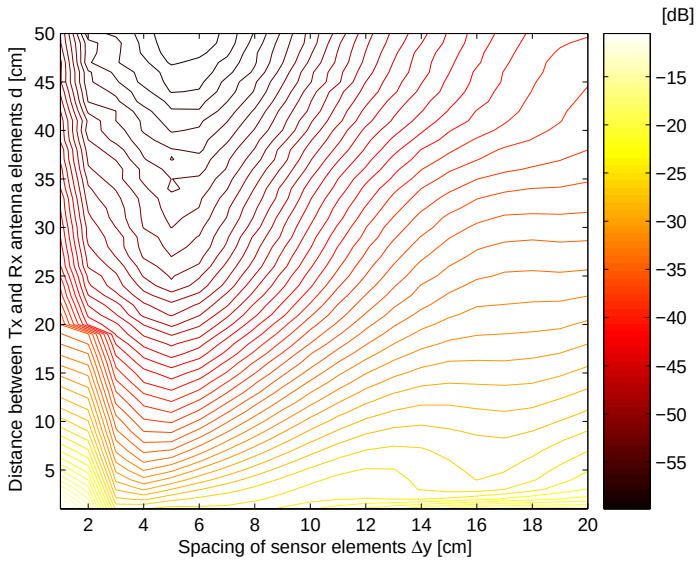


Figure 6.2: The power level inside the head as a 2-dimensional cost function $J(\Delta y, d)$ with respect to the spacing between the sensor elements and the distance between the transmitting and receiving antennas. These power levels refer to a system with N=5 sensor elements and M=2 actuator elements.

should be about 25 cm or more. This would result in a MIMO antenna system with a size of approximately 25 by 20 cm which is not practical to place on top of a mobile phone. Studying figure 6.2 and figure 6.3 we observe that if the original positions of the antenna elements, with an actuator antenna spacing of 2 cm is used and we increase the spacing of the sensor elements from 2 cm to 3 cm we would get an extra 3 dB attenuation inside the head compared to the original positioning of the antenna elements in figure 2.1. We have also investigated the impact on the systems performance as a result of changing the number of antenna elements in the actuator and sensor arrays. In these simulations we have calculated the least mean square solution as a function of the number of antenna elements in the actuator array M and the sensor array N.

Figure 6.4 shows, as expected, a decrease in the power level inside the head as long as every new added sensor element cover more of the head. Although, when the sensor array extends outside the length of the human head we attain no further improvement in the attenuation. Another interesting observation from figure 6.4 is that if the number of actuator elements is larger than the number of sensor elements the system becomes unstable.

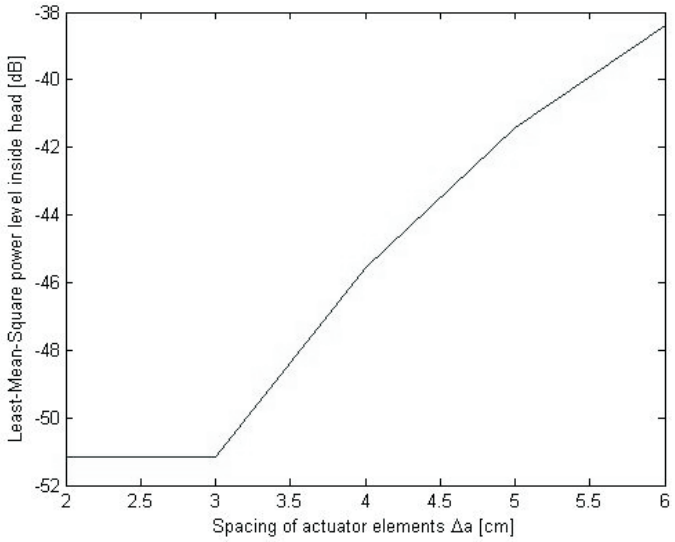


Figure 6.3: The effect of increasing the spacing $\Delta a$ between the actuator antenna elements. This result was calculated with a sensor array spacing of $\Delta y = 5$ cm and a separation between the sensor array and the actuator array of d = 25 cm.

Finally, we investigate the effect of the carrier frequency on the system performance. The suppression of the electromagnetic field inside the head so far in this report has been analyzed at the GSM frequency band centered at 900 MHz. Therefore, it would be interesting to investigate the effect of using this system at higher carrier frequencies in order to evaluate its performance at other GSM bands and the UMTS frequency band. In this experiment, we sweep the carrier frequency of the simulated system between 500 MHz and 2.5 GHz and the results can be viewed in figure 6.5. From this figure it can be clearly seen that we have a minimum point at the carrier frequency of 950 MHz. This optimum frequency is dependent on the type and size of the different antenna elements. It can also be noted from figure 6.5 that the attenuation of the power level at GSM/UMTS frequencies does not differ by more than 3-4 dB's.

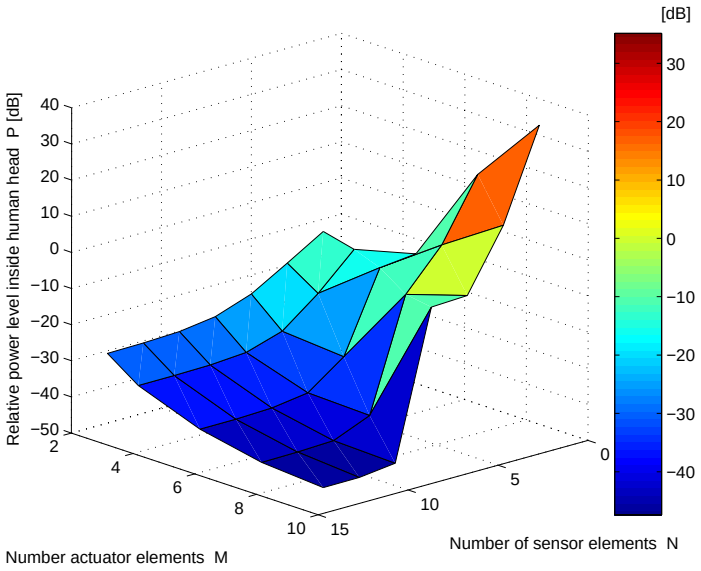


Figure 6.4: The relative power level in dB's as a function of the number of elements in the actuator and sensor array.

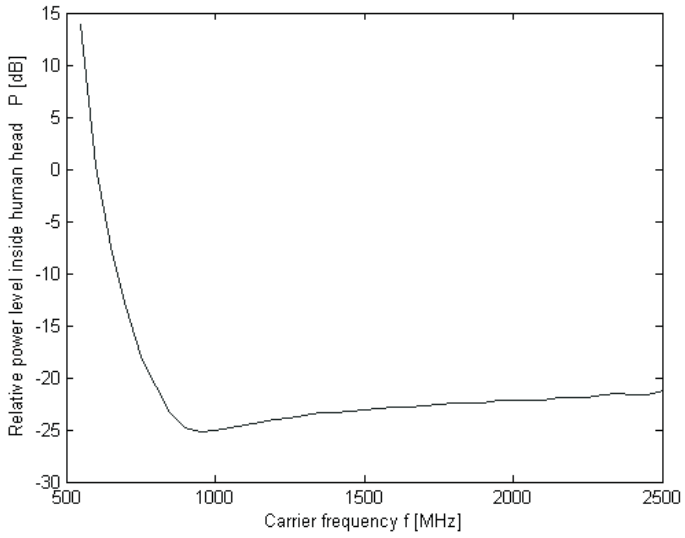


Figure 6.5: The change in power level inside the human head at different carrier frequencies. This simulation was done with a sensor array spacing of $\Delta y = 3$ cm and a distance between the sensor array and the actuator array of d = 3 cm.

# Chapter 7

# Conclusions

In this report we have presented a FEMLAB model which solves the partial differential equation of an electromagnetic field and simulated the physical MIMO antenna system which is controlled by various adaptive signal processing algorithms in order to suppress the field at a certain volume in space. We have also presented the solution for constraining the total output power of the system to a predefined level. In addition, we have investigated the effects of the size and number of MIMO antenna elements on the performance of the system and also tested the algorithms at different carrier frequencies. The attenuation levels achieved from these simulations suggest the possibility of using an active antenna system for this purpose although there are some practical difficulties in implementing these antenna arrays. In future work it would be interesting to extend this work into a 3D model and also to calculate the SAR value and the temperature increase in the brain tissue. Investigating the optimal type of antenna to be used in the different arrays would also be another interesting topic.

# Bibliography


[1] H.C. Christensen, J. Schüz, M. Kosteljanetz, H.S. Poulsen, J. Thomsen and C. Johansen, *Cellular Telephone and Risk of Acoustic Neuroma*, American Journal of Epidemiology, Volume 159, Number 3, pp 277-283, 2004.

[2] H. Lai, *Neurological Effects of Radiofrequency Electromagnetic Radiation*, Workshop on Possible Biological and Health Effects of RF Electromagnetic Fields, Mobile Phone and Health Symposium, 25-28 October 1998.

[3] Z.J. Sienkiewicz and C.I. Kowalczuk, *A Summary of Recent Reports on Mobile Phones and Health (2000-2004)*, National Radiological Protection Board Report, January 2005.

[4] T. Hult and A. Mohammed, *Suppression of EM Fields using Active Control Algorithms and MIMO Antenna System*, Radioengineering Journal, September, Volume 13, Number 3, pp 22-25, 2004.

[5] T. Hult and A. Mohammed, *Power Constrained Active Suppression of Electromagnetic Fields Using MIMO Antenna System*, invited paper in Journal of Communications Software and Systems (JCOMSS), November, Volume 1, Number 1, 2005.

[6] T. Hult and A. Mohammed, *The impact of MIMO Antenna System and Carrier Frequency on Active Control Suppression of Electromagnetic Field*, Wireless Networking Symposium 2004, Austin TX USA, 20-22 October 2004.

[7] T. Hult and A. Mohammed, *Power Constrained Active Suppression of Electromagnetic Fields Using MIMO Antenna System*, 12th International Conference on Software, Telecommunications and Computer Networks, SoftCOM 2004, Co-sponsored by IEEE Communications Society, Split Croatia, 10-13 October 2004.

[8] T. Hult, A. Mohammed and S. Nordebo, *Active Suppression of Electromagnetic Fields using a MIMO Antenna System*, 17th International Conference on Applied Electromagnetics and Communications, ICECom 2003, Co-sponsored by IEEE Communications Society, Dubrovnik Croatia, 1-3 October 2003.

[9] COMSOL AB, FEMLAB Electromagnetics module (Version 3.1).

[10] COMSOL AB, FEMLAB Reference Manual (Version 3.1).

[11] Y.W. Kwon and H.C. Bang *The Finite Element Method using MATLAB*, CRC Press LLC, 2000.

[12] O. Brander *Vektoranalys Modellering av fysikaliska problem i tre dimensioner*, Studentlitteratur, 1995.

[13] D.K. Cheng *Field and Wave Electromagnetics*, Addison-Wesley publishing company, 1989.

[14] G. Kristensson *Spridningsteori med antenntillmpningar*, Studentlitteratur, 1999.

[15] G. Stephenson and P.M. Radmore *Advanced mathematical methods for engineering and science students*, Cambridge University Press, 1990.

[16] C. Gabriel, *Compilation of the Dielectric Properties of Body Tissues at RF and Microwave Frequencies* Brooks Air Force Technical Report AL/OE-TR-1996-0037.

[17] B. Widrow, S.D. Stearns *Adaptive Signal Processing*, Prentice-Hall, 1985.

[18] S. Johansson *Active Control of Propeller-Induced Noise in Aircraft*, Doctoral Thesis, Blekinge Institute of Technology, 2000.

[19] M.H. Hayes *Statistical Digital Signal Processing and modeling*, John Wiley & Sons Inc, 1996.

[20] R. Fletcher *Practical Methods of Optimization*, John Wiley & Sons Ltd, 2000.

[21] S.M. Kuo, D.R. Morgan *Active Noise Control Systems*, John Wiley & Sons Inc, 1996.

[22] Z. Tian, K.L. Bell, and H.L. Van Trees *A Recursive Least Squares Implementation for Adaptive Beamforming Under Quadratic Constraint* Proceedings of 9th IEEE Signal Processing Workshop on Statistical Signal and Array Processing, Portland OR USA, pp. 9-12, September 1998.

# NOVEL APPLICATIONS OF MIMO ANTENNA SYSTEM FOR ACTIVE SUPPRESSION OF ELECTROMAGNETIC FIELDS

Tommy Hult och Abbas Mohammed


Printed by Kaserntryckeriet AB, Karlskrona 2005.

ISSN 1101-1581
ISRN BTH-RES–11/05–SE